WATER RESOURCES RESEARCH, VOL. 28, NO. 3, PAGES 939–950, MARCH 1992

Gravity-Driven Groundwater Flow and Slope Failure Potential 2. Effects of Slope Morphology, Material Properties, and Hydraulic Heterogeneity

MARK E. REID[1] AND RICHARD M. IVERSON

U.S. Geological Survey, Cascades Volcano Observatory, Vancouver, Washington

Hillslope morphology, material properties, and hydraulic heterogeneities influence the role of groundwater flow in provoking slope instability. We evaluate these influences quantitatively by employing the elastic effective stress model and Coulomb failure potential concept described in our companion paper (Iverson and Reid, this issue). Sensitivity analyses show that of four dimensionless quantities that control model results (i.e., Poisson's ratio, porosity, topographic profile, and hydraulic conductivity contrast), slope profiles and hydraulic conductivity contrasts have the most pronounced and diverse effects on groundwater seepage forces, effective stresses, and slope failure potentials. Gravity-driven groundwater flow strongly influences the shape of equilibrium hillslopes, which we define as those with uniform near-surface failure potentials. For homogeneous slopes with no groundwater flow, equilibrium hillslope profiles are straight; but with gravity-driven flow, equilibrium profiles are concave or convex-concave, and the largest failure potentials exist near the bases of convex slopes. In heterogeneous slopes, relatively slight hydraulic conductivity contrasts of less than 1 order of magnitude markedly affect the seepage force field and slope failure potential. Maximum effects occur if conductivity contrasts are of four orders of magnitude or more, and large hydraulic gradients commonly result in particularly large failure potentials just upslope from where low-conductivity layers intersect the ground surface.

INTRODUCTION

Gravity-driven groundwater flow in saturated hillslopes produces seepage forces that vary in magnitude and direction. These spatially variable seepage forces combine with uniform gravity and buoyancy forces to cause slope deformation, even in the absence of tectonic forces. The relationship between groundwater flow, effective stresses, and deformation that may lead to slope failure is not always obvious, however. Consequently, in a companion paper [*Iverson and Reid*, this issue] (hereafter referred to as Part 1) we formulated a linear poroelastic model of effective stresses and infinitesimal deformations in hillslopes with steady groundwater flow. We implemented the model using two finite element codes and analyzed the influence of gravity-driven groundwater flow on effective stresses in a straight, homogeneous hillslope. We also introduced the concept of a Coulomb slope failure potential, which characterized the potential for frictional instability in each element of the slope. Our results illustrated some fundamental effects of groundwater flow on slope stability, and they established a framework for addressing the more complex situations that exist in natural hillslopes.

Natural hillslopes exhibit a wide range of geologic and hydrologic characteristics. Hillslope materials include rocks and soils with diverse physical properties, and slopes have a variety of topographic profiles. Commonly, natural hillslopes have rock or soil layers with differing hydraulic conductivities. These heterogeneities may strongly influence groundwater flow and lead to locally large seepage forces. All these factors may, in turn, influence the effective stress distribution in the hillslope and thereby control the location of areas with large slope failure potentials.

In this paper we determine the distributions of seepage force, elastic effective stress, and Coulomb failure potential in hillslopes with a variety of topographic profiles, material properties, and hydraulic heterogeneities. We focus especially on modifications of failure potential that result from groundwater flow. Although many previous studies indicate a correlation between excess pore pressures (i.e., pressure deviations from hydrostatic, which drive groundwater flow) and slope failure, they do not investigate the effective stress field modifications caused by the excess pore pressure distribution [e.g., *Reid et al.*, 1988]. We investigate these groundwater effects by including spatially variable seepage forces in our effective stress analysis.

Throughout our analysis, we use the same governing equations, boundary conditions for periodic topography, and finite element modeling approach described in Part 1. By conducting a systematic sensitivity analysis of model results we address important questions such as: do the material properties of a hillslope strongly influence effective stresses and failure potential?; do certain hillslope geometries have higher failure potentials than others?; and what types of hydraulic heterogeneities produce seepage forces that lead to particularly large failure potentials? We begin by explaining our use of the failure potential Φ and by examining the effects of variations in Poisson's ratio ν, bulk density ρ_t, and hillslope shape on effective stresses and failure potentials in saturated, homogeneous hillslopes. Then we assess the effects of spatially variable hydraulic conductivities on the distributions of seepage force, effective stress, and failure potential. Finally, we discuss how these effects may influence the location of slope failures and the geomorphology of regions sculpted by mass movements.

[1]Now at U.S. Geological Survey, Honolulu, Hawaii.

Paper number 91WR02695

FAILURE POTENTIAL

Shear failure of cohesionless earth materials is described well by the Coulomb failure rule:

$$\frac{\sigma_1 - \sigma_3}{\sigma_1 + \sigma_3} = \frac{|\tau'_{max}|}{-\sigma'_m} = \sin \phi \qquad (1)$$

where σ_1 and σ_3 are the maximum and minimum principal effective stresses, respectively; τ'_{max} is the maximum shear stress; σ'_m is the mean effective normal stress (positive in tension); and ϕ is the angle of internal friction (Part 1). We can evaluate the stress ratio $|\tau'_{max}|/(-\sigma'_m)$ without knowledge of the angle of internal friction, and we consequently define the quantity

$$\Phi = |\tau'_{max}|/(-\sigma'_m) \qquad (2)$$

as a dimensionless measure of the shear failure potential at any point. In hillslopes with significant spatial variations in ϕ, values of Φ provide an imprecise measure of the relative failure potential at different points. However, in hillslopes with uniform ϕ, Φ provides an accurate index of the relative failure potential. Owing to our focus on groundwater effects and our desire to avoid the complicating influences of strength heterogeneity, we use Φ values extensively to assess distributions of slope failure potential (cf. Part 1).

HOMOGENEOUS HILLSLOPES

In our effective stress model the governing equations contain five parameters, which have values that may differ between various homogeneous hillslopes. These parameters include K, the hydraulic conductivity, in the equation for steady state, saturated groundwater flow (equation (15) in Part 1) and Poisson's ratio ν, Young's modulus E, pore water density ρ_w, and bulk mixture density ρ_t in the equations for elastic displacement (equation (17) in Part 1). For a saturated hillslope composed of homogeneous, isotropic material and for the boundary conditions we use, the value of the hydraulic conductivity, K, does not influence the hydraulic head distribution. It also does not affect the seepage force field (specified by $-\rho_w g \nabla h$, where h is hydraulic head and g is the magnitude of gravitational acceleration) that influences the elastic effective stresses. Thus in this case the value of K does not influence the failure potential of the hillslope.

In homogeneous porous media, only two of the four parameters in the elastic displacement equations are independent of one another and influence the effective stress distribution. Although E appears in the displacement equations, the use of Hooke's law for a homogeneous, isotropic, linearly elastic material eliminates E from the stress solution (see Part 1). Thus only one elastic parameter ν influences the effective stress distribution and failure potential. Bulk density ρ_t can vary with the densities of the solid and fluid phases as well as the porosity n of the material. However, if we assume that the solid, ρ_s, and fluid, ρ_w, densities are constant, then only the porosity n is required to calculate ρ_t for both dry and saturated hillslopes:

$$\text{dry } \rho_t = (1 - n)\rho_s \qquad (3a)$$

$$\text{saturated } \rho_t = (1 - n)\rho_s + n\rho_w \qquad (3b)$$

TABLE 1. Typical Properties of Earth Materials

Material	Poisson's Ratio, ν	Porosity, n	Hydraulic Conductivity,§ K, m/s
Soils*	0.28–0.333	0.1–0.6	10^{-2}–10^{-7}
Sedimentary Rocks	0.1–0.3†	0.01–0.25‡	10^{-6}–10^{-10}
Crystalline Rocks	0.1–0.25†	low	10^{-10}–10^{-13}

*Data are from *Lambe and Whitman* [1979].
†Data are from *Birch* [1966] and *Jaeger and Cook* [1979].
‡Data are from *Daly et al.* [1966].
§Data are from *Freeze and Cherry* [1979].

Thus for a homogeneous, isotropic material, the controlling physical parameters are ν and n. Typical values of these parameters for rocks and soils are shown in Table 1. We focus initially on the effects of these two parameters; then we examine effects of variations in slope inclination and morphology. Our results are nondimensionalized as described in Part 1.

Effect of Poisson's Ratio

Poisson's ratio ν for soils and rocks commonly ranges between 0.1 and 0.333 (Table 1). The coefficient of lateral earth pressure, K_e, commonly used in soil mechanics is related to the elastic Poisson's ratio ν by [*Dunn et al.*, 1980]:

$$K_e = \nu/(1 - \nu) \qquad (4)$$

Thus the K_e value of 0.5, commonly used for normally consolidated soil [*Lambe and Whitman*, 1979] is equivalent to a ν value of 0.333.

Using finite element models (described in Part 1), we analyze the influence of ν on the elastic effective stress field and Coulomb failure potential in a straight hillslope with an inclination of 26.6° and a porosity n of 0.1 (a dry ρ_t of 2385 kg/m^3, and a saturated ρ_t of 2485 kg/m^3). We use three values of ν: 0.1, 0.25, and 0.333. Table 2 summarizes the hillslope properties used in these simulations as well as those used in the other simulations described in this paper.

As the value of ν increases, stresses acting in one direction have more influence on stresses acting in other directions, and the vertical gravitational force induces more lateral expansion in response to vertical contraction. Accordingly, the magnitudes of the two principal stresses, σ_1 and σ_3, become more equal as ν increases. This, in turn, decreases shear stresses and the hillslope failure potential. Figure 1 shows this effect for a material element near the surface of a dry, elastic hillslope. The reduction in Φ is also present in saturated hillslopes. For three saturated hillslopes with different values of ν, Figure 2 shows regions with a failure potential Φ greater than 0.7. A small region of lateral tensile stress exists near the toe of the slope in the case with $\nu = 0.1$. As ν increases, the zone of tension disappears and the extent of regions with large Φ decreases. It is clear from these results that ν strongly influences the extent of regions with a large failure potential.

Figure 3 shows contours of the percent increase in Φ between dry and saturated hillslopes for the three different Poisson's ratios considered in Figure 2. This change in Φ is significant because it shows the influence of ν on the extent to which groundwater seepage modifies the effective stress

TABLE 2. Summary of Hillslope Properties Used to Generate Model Results

Hillslope Property:	ν	n	Inclination	Morphology	Heterogeneity ($\log_{10}$ of K contrast)	Figures Showing Results
			Homogeneous Hillslopes			
Effects of:						
Poisson's Ratio, ν	0.1	0.1	26.6° (2:1)	straight	0	1, 2, 3
	0.25	0.1	26.6° (2:1)	straight	0	1, 2, 3
	0.333	0.1	26.6° (2:1)	straight	0	1, 2, 3
porosity, n	0.333	0.01	26.6° (2:1)	straight	0	4, 5
	0.333	0.1	26.6° (2:1)	straight	0	4, 5
	0.333	0.25	26.6° (2:1)	straight	0	4, 5
	0.333	0.4	26.6° (2:1)	straight	0	4, 5
inclination	0.333	0.1	45° (1:1)	straight	0	6
	0.333	0.1	26.6° (2:1)	straight	0	6
	0.333	0.1	18.4° (3:1)	straight	0	6
morphology	0.333	0.1	26.6° (2:1)	straight	0	7, 8
	0.333	0.1	26.6° (2:1)	convex	0	7, 8
	0.333	0.1	26.6° (2:1)	concave	0	7, 8
	0.333	0.1	26.6° (2:1)	convex-concave	0	7, 8
			Heterogeneous Hillslopes			
Effects of:						
slope-parallel layer	0.333	0.1	26.6° (2:1)	straight	+4	12
	0.333	0.1	26.6° (2:1)	straight	−0.7	12
horizontal layer	0.333	0.1	26.6° (2:1)	straight	+1	13
	0.333	0.1	26.6° (2:1)	straight	−1	13
vertical layer	0.333	0.1	26.6° (2:1)	straight	+4	14
	0.333	0.1	26.6° (2:1)	straight	−4	14

state and failure potential of the hillslope. The overall percent increase in Φ is smallest in hillslopes with small values of ν (0.1). In hillslopes with $\nu = 0.25$ and 0.333 the percent increase is greater because the effective stress state is more nearly spherical (i.e., $\sigma_3 \rightarrow \sigma_1$) and the role of groundwater flow in producing deviatoric stresses is more significant. However, the percent increase in Φ for these two cases is very similar. Thus for our subsequent analyses our choice of ν in the range 0.25–0.33 is relatively unimportant because we are interested primarily in the extent to which gravity-driven groundwater flow modifies the failure potential in a hillslope and not in the absolute magnitude of Φ.

Effect of Porosity

The porosity n of rocks and soils ranges from less than 0.01 to over 0.6 (Table 1). If we assume typical densities for the pore water, ρ_w, of 1000 kg/m^3 and for the solids, ρ_s, of 2650 kg/m^3, then we can calculate the dry ρ_t and saturated ρ_t for any porosity using (3*a*) and (3*b*). Table 3 shows the bulk densities corresponding to selected values of porosity. Using finite element models, we compute the influence of differences in porosity (and therefore in ρ_t) on the failure potential in a straight hillslope having $\nu = 0.333$ and the properties shown in Table 2. We use dry and saturated bulk densities corresponding to n values of 0.01, 0.1, 0.25, and 0.4.

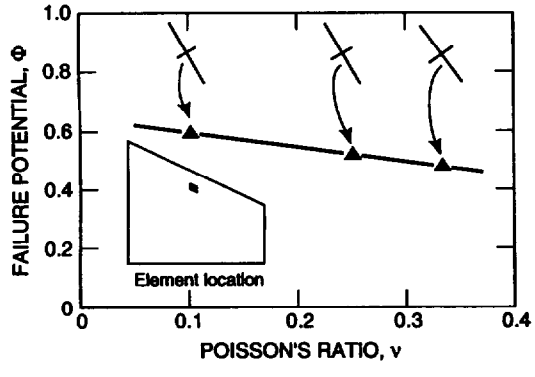

Fig. 1. Failure potential Φ as a function of Poisson's ratio ν at element shown in dry hillslope. Orientation and relative magnitude of principal stresses in the element are shown for three ν values.

For dry hillslopes an increase in n (or decrease in ρ_t) decreases the gravitational body force and thereby decreases the magnitudes of the two principal stresses. However, both stresses are decreased by a proportional amount, their orientation remains the same, and the failure potential Φ consequently remains the same throughout the hillslope. Figure 4 illustrates this effect for a selected element near the surface of the slope.

In contrast, the magnitude and orientation of the principal effective stresses as well as the Coulomb failure potential differ between saturated hillslopes with different values of n. Figure 5 shows regions with a failure potential greater than 0.7 for saturated hillslopes having $n = 0.01$, 0.25, and 0.4 ($n = 0.1$ is shown in Figure 2). These regions become somewhat larger, especially near the toe of the slope, as n increases. Because the seepage forces ($-\rho_w g \nabla h$) are not affected by ρ_t, they remain constant as porosity increases. However, the gravitational body force that acts on the solids decreases as ρ_t decreases and n increases. Therefore the effects of the seepage forces become more prominent as porosity increases. In spite of the fact that n increases by more than an order of magnitude, the change in failure potential shown in Figure 5 is relatively small.

Effect of Slope Inclination

Depending on material strength, gravity-induced landsliding can occur on virtually any slope inclined above horizon-

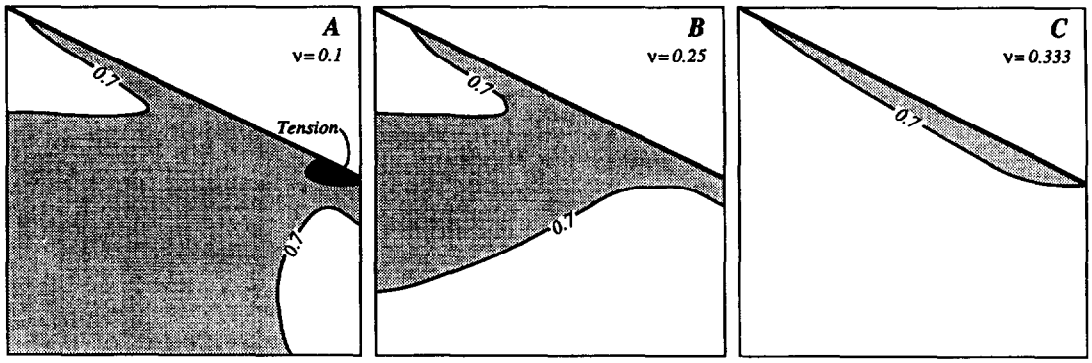

Fig. 2. Shading shows regions with failure potential Φ greater than 0.7 in saturated hillslopes with differing values of Poisson's ratio ν.

tal. However, subaerial landslides typically occur under a more limited range of inclinations. For example, *Campbell* [1975] noted that shallow soil slips are common on natural slopes with a horizontal-to-vertical (H:V) ratio between 3:1 (18.4°) and 1:1 (45°). We investigate the effective stress distribution and failure potential in straight hillslopes with three different angles of inclination: 18.4°, 26.6°, and 45°. All three hillslopes have a nondimensional height of one. Table 2 lists the other relevant hillslope properties.

For all three inclinations the overall groundwater flow, effective stress, and failure potential patterns are similar to those for the straight, homogeneous, 2:1 (26.6°) hillslope discussed in Part 1. In all cases the largest Φ values occur in the near-surface region, and Φ values increase with the addition of gravity-driven groundwater flow. Figure 6 shows the normalized seepage forces (specified by $-\nabla h$) and contours of Φ greater than 0.7 for the three saturated hillslopes with different inclinations. In all three the patterns are similar and Φ values are largest near the toe of the slope, where flow is upward and outward. In the steeper slopes the near-surface compressive stresses oriented subparallel to the ground surface become larger, and consequently near-surface Φ values increase.

Effect of Slope Morphology

Natural hillslopes have a variety of shapes that result from diverse bedrock lithology and structure, climate and vegetation, and geologic histories. Straight, convex, concave, and combination convex-concave slope profiles are all common [*Carson and Kirkby*, 1972]. Although the topography in our model is constrained to be periodic by the boundary conditions described in Part 1, the shape of the upper boundary representing the ground surface may vary. We use four different slope profiles, described by the equations in Table 4, to investigate the effects of differences in slope morphology on the groundwater flow pattern and the effective stress distribution within a hillslope. For our simulations the overall slope is 2:1, and the slope's physical properties are listed in Table 2.

Figure 7 shows contours of failure potential Φ for dry hillslopes having the four different profiles. In all cases the value of Φ is largest near the surface. Although Φ values are nearly uniform near the surface in the straight slope, they vary in the other profiles. Φ values are largest near the toe of the slope in the convex slope, in the upper midslope in the concave slope, and in the steep midslope section of the convex-concave slope. In these cases, Φ values are generally the largest in the steepest sections of the slope, provided they are relatively distant from the lateral boundaries.

When the slope is saturated with flowing groundwater, the patterns and magnitudes of failure potential change. Figure 8 illustrates the normalized seepage force vectors and contours of Φ for the saturated slopes. The pattern of near-surface Φ values can be interpreted by examining the interaction of the local topographic steepness and the direction and magnitude of near-surface groundwater seepage forces. In the convex profile the seepage force vectors are large and oriented outward from the slope in the steep toe region. Here both the local steepness and the flow direction combine to create a region of tensile stresses as well as large values of Φ.

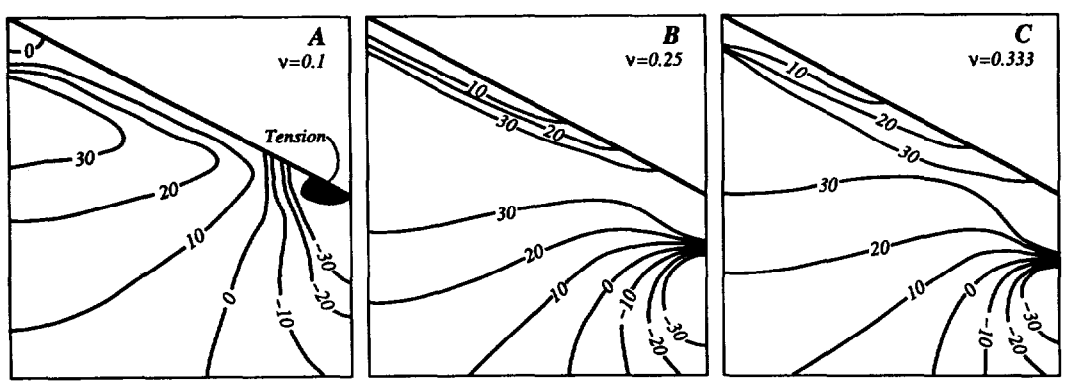

Fig. 3. Percent increase in failure potential Φ between dry and saturated hillslopes for differing Poisson's ratio ν.

TABLE 3. Porosity and Bulk Density Variation

Porosity, n	Dry, ρ_t/ρ_w	Saturated, ρ_t/ρ_w
0.01	2.62	2.63
0.1	2.38	2.48
0.25	1.99	2.24
0.4	1.59	1.99

Computed densities are based on the values $\rho_w = 1000$ kg/m^3 and $\rho_s = 2650$ kg/m^3.

In the concave profile, Φ values are generally more uniform near the surface, with a local high-Φ region in the midslope. Here flow subparallel to the slope acts to expand the region of high Φ values relative to that in the dry hillslope. In the convex-concave profile, Φ values are large and nearly uniform in the steeper near-surface region. In both the concave and convex-concave profiles, groundwater flow is downward or subparallel to the slope in the steeper midslope section and outward at the less-steep toe. This outward flow at the toe compensates for the lack of steepness and increases the Φ values, creating a more uniform near-surface distribution of Φ.

HETEROGENEOUS HILLSLOPES

Most natural hillslopes are composed of stratified earth materials with different physical properties. This stratification, resulting from diverse geologic processes, can take many forms, including slope-parallel surficial deposits or weathering products overlying rock, nearly horizontal layers of sedimentary or volcanic rocks, or nearly vertical, dikelike intrusions. The hydraulic conductivity K of geologically dissimilar soils and rocks ranges over roughly 11 orders of magnitude, and for apparently similar materials it may range over 3 or 4 orders of magnitude (Table 1) [*Iverson and Major*, 1987]. Contrasts in the hydraulic conductivity of layered materials can profoundly modify the groundwater flow field [cf. *Freeze and Witherspoon*, 1967] and create locally large seepage forces.

To examine the influence of stratified materials on slope failure potential, we use three layered configurations with a straight 2:1 slope profile: a slope-parallel layer, a horizontal layer, and a vertical layer (Figure 9). A straight profile eliminates stress modifications induced by local variations in slope angle. In each case the layer has a hydraulic conductivity that differs from that of the surrounding materials. In steady state groundwater flow systems the contrast in K values between materials, not the magnitude of K, affects the hydraulic head distribution. Moreover, although the magnitude of K greatly affects the Darcian flow velocity (given by $-K\nabla h$), it does not affect the seepage force (given by $-\rho_w g\nabla h$). Therefore we restrict our attention to the hydraulic conductivity contrast between the layer and the surrounding material.

Cases A and B in Figure 10 show the normalized seepage force vectors in two hillslopes having a layer with a higher hydraulic conductivity parallel to the slope profile. In case A the conductivity of the layer is only 1 order of magnitude greater than that of the underlying material, whereas in case B the conductivity of the layer is 4 orders greater. In both hillslopes the flow pattern is significantly different from that in the homogeneous hillslope (compare with Figure 8). In the layered cases, flow in the upper layer is subparallel to the slope profile. Flow velocity vectors (not shown in the figure) increase proportionally as the hydraulic conductivity of the layer increases. Thus flow velocities in the high-conductivity layer are orders of magnitude larger than in the underlying low-conductivity material. However, even with greatly different hydraulic conductivity contrasts in cases A and B, the overall seepage force field is surprisingly similar. It is the seepage force field, not the flow velocity field, that influences the elastic effective stress field and failure potential.

Cases C and D illustrate the seepage force vectors in two hillslopes having a vertical low-conductivity layer. Case C has a layer 1 order of magnitude lower than the surrounding material; case D has a layer 4 orders lower. As with the slope-parallel layer, the seepage force field in these two cases is very similar, although the vectors are somewhat larger in case D. Two aspects of the seepage force field in both these layered hillslopes are particularly interesting: (1) even a small hydraulic conductivity contrast significantly modifies the seepage force field, and (2) a larger conductivity contrast modifies the seepage force field in a manner similar to that of a smaller contrast. These two aspects are common to all our hillslope seepage force fields with slope-parallel, horizontal, or vertical layers.

Because seepage forces are derived directly from the hydraulic head distribution, we examine this distribution to ascertain differences between layered hillslopes with different hydraulic conductivity contrasts. Figure 11 shows the maximum change in hydraulic head induced by different K contrasts; these changes are relative to a homogeneous hillslope. For each of the three layer geometries we consider the maximum hydraulic head change is largest for large conductivity contrasts. However, most of the head change occurs between no contrast and 3 or 4 orders of magnitude contrast. Greater contrasts have little effect on the maximum head change. For these cases our results indicate that a hydraulic conductivity contrast of 4 orders of magnitude ($\log_{10}(K_{layer}/K_{surrounding}) = \pm 4$) is sufficient to obtain the maximum change in seepage forces that can be induced by hydraulic heterogeneities. These large contrasts can lead to regions of large negative pressure head, indicating partially saturated conditions, in hillslopes with slope-parallel or horizontal layers. Our model does not account for partially saturated conditions (cf. Part 1).

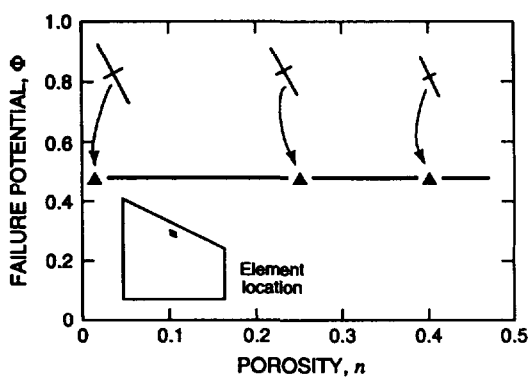

Fig. 4. Failure potential Φ as a function of porosity n at element shown in dry hillslope. Orientation and relative magnitude of principal stresses in the element are shown for three n values.

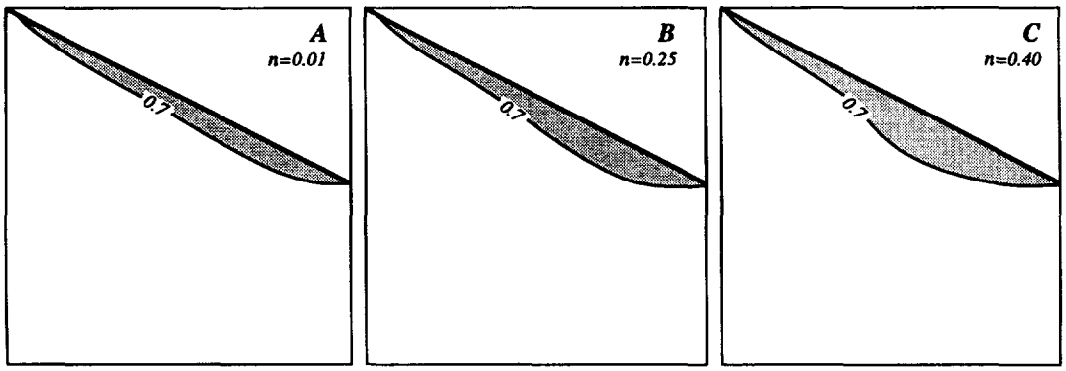

Fig. 5. Shading shows regions with failure potential Φ greater than 0.7 in saturated hillslopes with differing porosity n.

As a consequence of these findings, we use a K contrast of 4 orders of magnitude for three cases: a high-conductivity slope-parallel layer, a high-conductivity vertical layer, and a low-conductivity vertical layer. To maintain positive pressure heads throughout the flow domain, we use lower conductivity contrasts in the other three cases (low-conductivity slope-parallel layer, both low- and high-conductivity horizontal layers). Although physical properties other than hydraulic conductivity may vary with layering, our simulations use a uniform ν equal to 0.333 and n equal to 0.1 throughout the hillslope (Table 2). Compared with other possible values (shown in Table 1), these values of ν and n are conservative in that they tend to minimize the effects of seepage forces. Thus our simulations illustrate the maximum effects induced by hydraulic conductivity contrasts, while minimizing the influences of ν and n.

Slope-Parallel Layer

To investigate the failure potential of heterogeneous hillslopes with a layer that parallels the slope surface, we analyze two cases: one with a layer hydraulic conductivity that is 4 orders of magnitude higher than that of the underlying material, the other with a layer conductivity that is 5 times lower. Figure 12 shows the seepage force vectors and contours of Φ greater than 0.7 for these two cases. With the higher-K layer (case A), groundwater flow throughout much of the layer is subparallel to the slope surface. This flow pattern is very similar to that assumed in the commonly used infinite slope, limit equilibrium slope stability model with slope-parallel flow [e.g., *Skempton and Delory*, 1957]. This flow pattern has also been hypothesized to occur in shallow soil slips [*Campbell*, 1975]. In the underlying region, flow is similar to that in the homogeneous hillslope. The value of Φ is highest and approximately uniform near the surface of the slope-parallel layer.

With the lower-K layer parallel to the slope (case B) the seepage force field differs from those in both the higher-K layer hillslope (case A) and the homogeneous hillslope. Here seepage forces are large in the slope-parallel layer, oriented downward in the upslope portion and upward in the downslope portion of the slope. Seepage forces in the underlying material with higher K are smaller. The downslope portion of the layer has very large Φ values. This case exhibits substantially higher failure potentials than either case A or the homogeneous case.

Horizontal Layer

In hillslopes having a horizontal layer with a hydraulic conductivity contrast of 1 order of magnitude, the seepage force patterns and Coulomb failure potentials differ from those in the hillslopes with a slope-parallel layer. With a higher-K horizontal layer (case A of Figure 13), seepage forces in the layer are small and directed outward near the ground surface. Above the layer in lower-K material, seepage forces are larger but directed vertically downward. Below the layer, seepage forces are similar to those in the homogeneous hillslope. The highest failure potential occurs in a thin zone near the surface in the layer and downslope of the layer where seepage forces are directed outward from the slope.

In case B (Figure 13) with a lower-K layer, seepage forces are very large in the layer but are directed downward. Above the layer, seepage vectors are oriented outward from the slope. Below the layer in the higher-K material, seepage forces are generally small, with some larger forces acting upward near the toe of the slope. Failure potential is highest where seepage forces are directed outward from the slope, above the layer and at the toe of the slope.

Vertical Layer

Seepage forces in a hillslope having a vertical layer of contrasting hydraulic conductivity differ markedly from those in the previous cases. Figure 14 shows the seepage-force vectors and contours of Φ for a higher-K vertical layer (case A) and for a lower-K vertical layer (case B). In case A with a higher-K layer, seepage forces are small in the layer. Much larger seepage forces occur in the surrounding lower-K material with an overall flow pattern similar to that in the homogeneous hillslope. Seepage force vectors are particularly large near the surface downslope of the layer. Φ is largest at the downslope edge of the vertical layer where large seepage forces are directed outward from the slope.

With a lower-K layer in case B, seepage forces are very large in the layer (hydraulic gradients exceed 1.0) and are directed horizontally. Seepage forces in the surrounding higher-K material are smaller except near the surface. On each side of the layer, flow circulates in nearly isolated cells. Seepage forces just upslope of the layer are large and directed outward from the slope. Because of this and the large horizontal seepage forces in the vertical layer, a large region of high Φ exists upslope of the vertical layer.

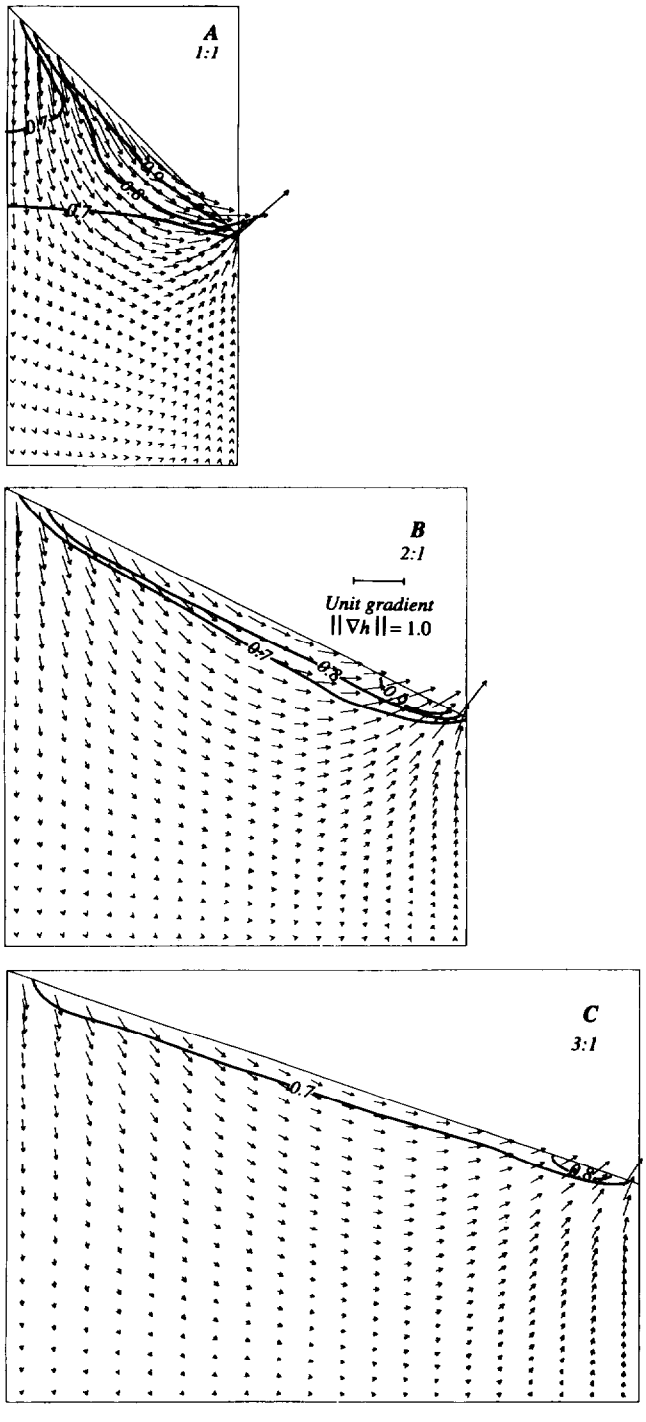

Fig. 6. Normalized seepage force vectors and contours of failure potential Φ greater than 0.7 in saturated hillslopes with differing slope inclinations: (*a*) 1:1; (*b*) 2:1; (*c*) 3:1.

DISCUSSION

Our model results show how hillslope morphology, material properties, and hydraulic heterogeneities can markedly affect the magnitude and distribution of the failure potential Φ within a saturated hillslope. As a consequence of gravity-driven groundwater flow, near-surface hillslope regions almost universally have an increased Φ in comparison to a dry hillslope. Material properties such as density ρ_t and Poisson's ratio ν can affect the change in Φ between dry and saturated hillslopes. However, in our examples, slope morphology and hydraulic heterogeneities have a much larger effect on Φ. These two factors can greatly modify both the seepage force field due to gravity-driven groundwater flow and the resulting effective stress field.

TABLE 4. Slope Profiles

Morphology	Profile Equation*
Straight	$y/H = 1-(x/L)$
Convex†	$y/H = 1-(x/L)^2$
Concave†	$y/H = 1-(x/L)^{0.5}$
Convex-concave‡	$y/H = \dfrac{1/9}{1/9 + (x/L)^2}$

*H is the hillslope height, measured vertically, and L is the hillslope length, measured horizontally.
†Equation modified from *Kirkby* [1971].
‡Equation modified from *McTigue and Mei* [1981].

Geomorphological Implications

The distribution of near-surface failure potential in hillslopes may have significant geomorphological consequences, particularly for landscapes sculpted primarily by mass movements. Other investigators have proposed that tectonically or gravitationally induced stress fields in steep mountainous regions can lead to the development of statically stable forms such as spurs, pyramids, and rounded convex pillars [*Gerber and Scheidegger*, 1969, 1975]. Although speculative, we can extend this line of reasoning further. If hillslope sections with locally high Φ are more prone to slope failure, then landsliding processes might be expected to alter the hillslope morphology. However, if a particular slope morphology has a uniform near-surface Φ, then this slope form may be more in equilibrium with the effective stress field affecting the domain. This, in turn, could result in fewer localized slope failures and a more stable morphology.

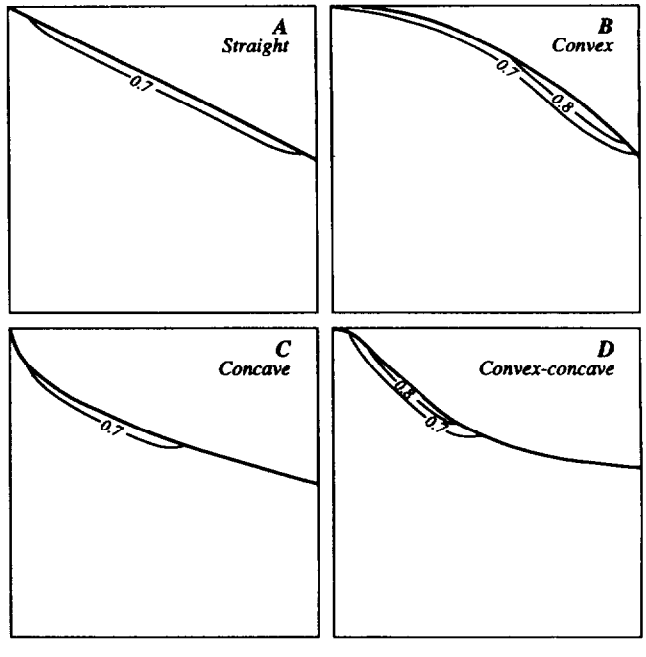

Fig. 7. Contours of failure potential Φ greater than 0.7 in dry hillslopes with differing slope morphology.

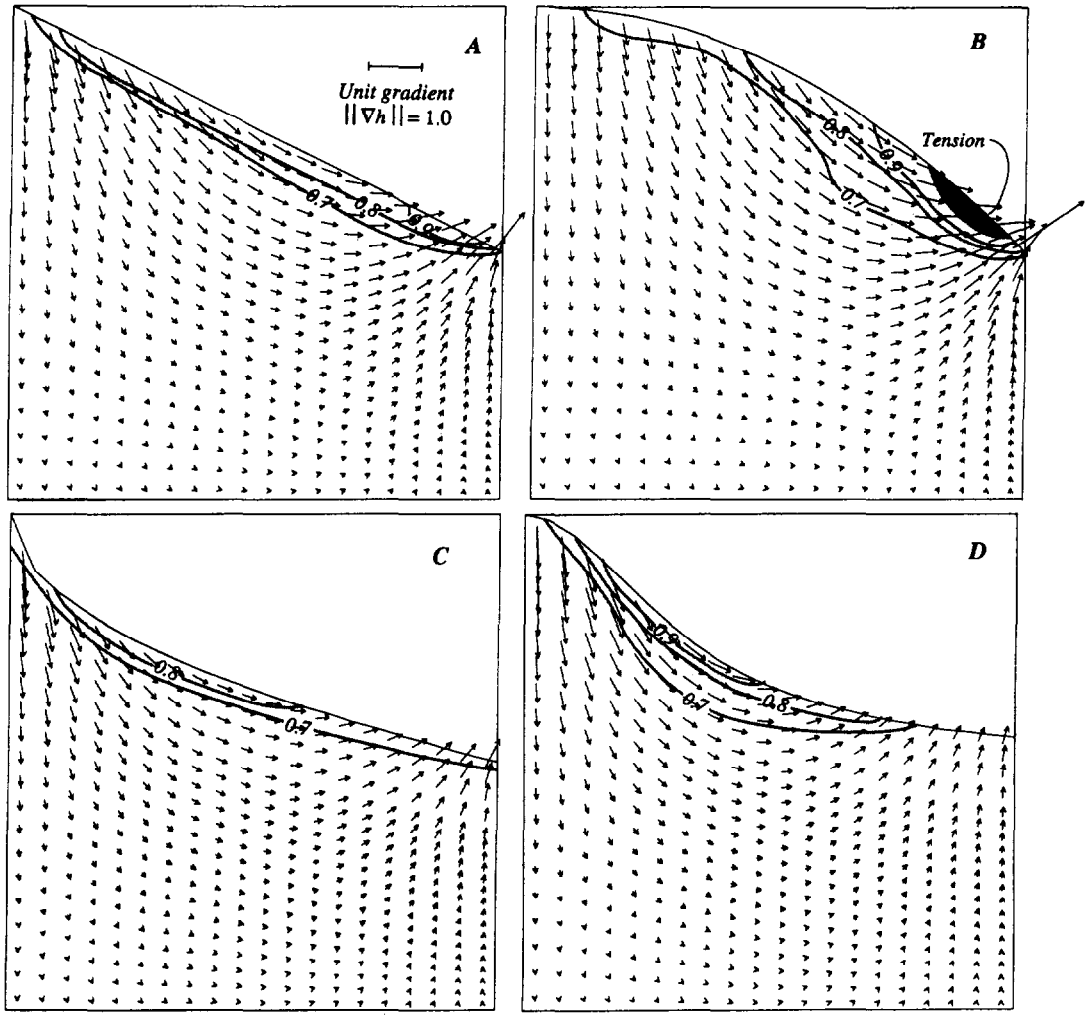

Fig. 8. Normalized seepage force vectors and contours of failure potential Φ greater than 0.7 in saturated hillslopes with the differing morphologies shown in Figure 7.

In saturated, homogeneous materials, the largest failure potentials occur in convex hillslopes where seepage forces are directed outward from the steep, lower section of the slope (see Figure 8). This convex form would be more prone to slope failure than the other forms we examined. Such convex profiles commonly occur in areas dominated by creep movement [*Carson and Kirkby*, 1972] and in areas of rapid tectonic uplift, where pronounced incision of the landscape by streams may lead to development of steep, streamside inner gorges [e.g., *Dutton*, 1882; *Kelsey*, 1988]. Gravity-driven groundwater flow and effective stress distributions may contribute to the instability of such inner gorges in humid regions by increasing the failure potential near the base of the gorge slopes.

When saturated with flowing groundwater, straight and convex hillslopes have near-surface regions of locally high

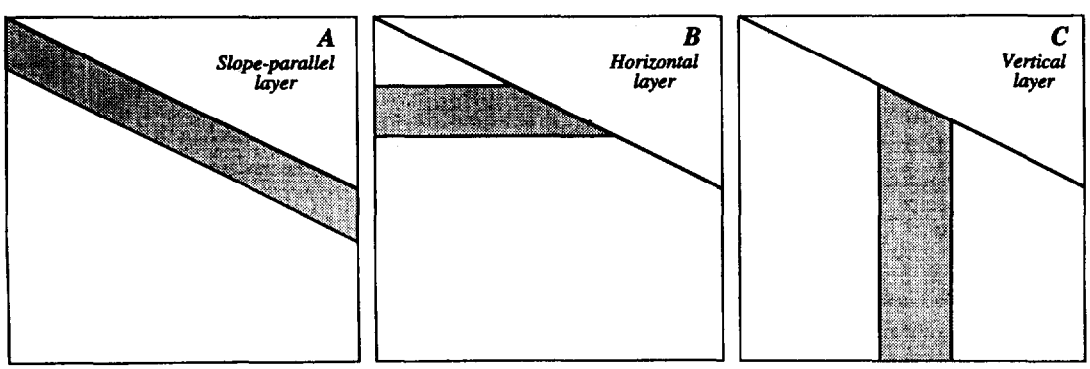

Fig. 9. Layer configurations for hydraulically heterogeneous hillslopes.

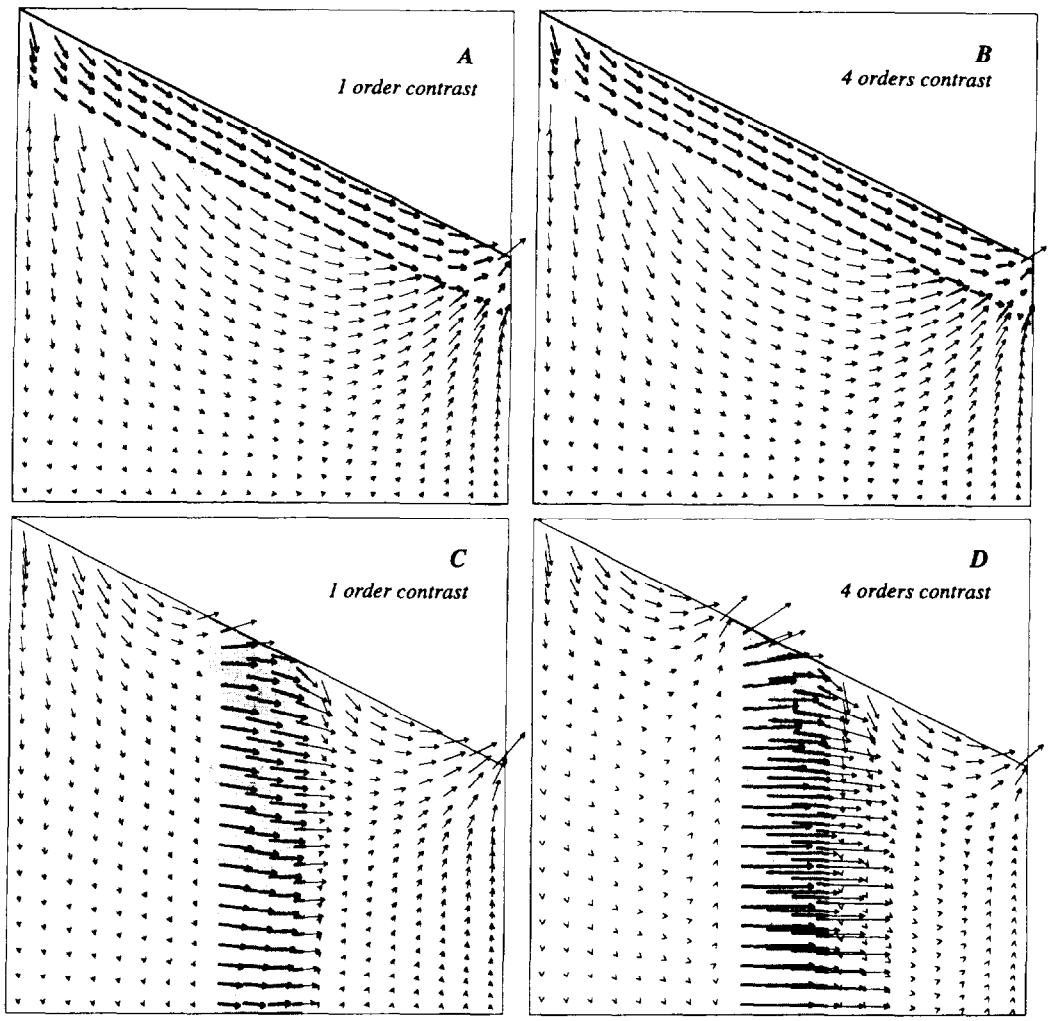

Fig. 10. Normalized seepage force vectors for selected heterogeneous hillslopes. (*a*) and (*b*) High-conductivity slope-parallel layers with K values 1 and 4 orders of magnitude greater than that of underlying material. (*c*) and (*d*) Low-conductivity vertical layers with K values 1 and 4 orders of magnitude less than that of adjacent material.

Φ. In contrast, concave and convex-concave hillslopes have a more uniform Φ near the ground surface (Figure 8). When dry, the straight form has a more uniform near-surface Φ (Figure 7). These results indicate that a straight form is more gravitationally stable in hillslopes without groundwater flow, whereas a concave or convex-concave form is more gravitationally stable for saturated hillslopes with gravity-driven groundwater flow. Thus mass movement processes such as dry ravel may lead hillslope profiles to evolve toward straight forms in arid regions where saturated groundwater flow is uncommon. Conversely, concave or convex-concave slopes would be the expected equilibrium forms in humid regions where hillslopes are nearly saturated with groundwater and are sculpted mainly by mass movements. These "favored" slope forms correspond with those most commonly observed in arid and humid environments, respectively [*Carson and Kirkby*, 1972].

Hydrogeological Implications for Slope Stability

In our examples, gravity-driven groundwater flow clearly affects the elastic effective stress field and can locally increase the hillslope failure potential. Thus any hydrogeological controls on the flow field can be expected to change the distribution of Φ. The greatest increase in Φ occurs when seepage is directed at an angle, λ, that is between zero and 90-θ deg, where θ is the slope angle and λ is measured with respect to an outward-directed surface-normal vector (see Part 1). This corresponds to seepage directed upward and outward from the slope. Thus conditions that create large seepage forces acting in these directions tend to create areas with large values of Φ.

In hydraulically homogeneous hillslopes, seepage forces are directed downward at the head of the slope and upward at the toe. Although this effect is enhanced near the lateral no-flow boundaries used in our model, it occurs in any gravity-driven groundwater flow system [cf. *Freeze and Witherspoon*, 1966, 1967]. These outwardly directed seepage forces tend to create a localized region of high Φ. Therefore a homogeneous hillslope of uniform steepness (i.e., a straight slope) has a higher Φ near the slope toe as a consequence of groundwater flow. Our results indicate that most discharge areas in a saturated hillslope have higher Φ than the corresponding region in the identical dry hillslope. Recharge areas have a similar Φ to that in the corresponding dry region.

Natural hillslopes, however, are rarely homogeneous. Typically, some geologic or pedologic stratification is present, in either or both the soil and the bedrock. Given even a relatively small hydraulic conductivity contrast between these layers, significant changes in the groundwater flow field and corresponding effective stress field result. In a layered system containing materials of higher and lower conductivity, larger hydraulic gradients and therefore larger seepage forces tend to occur in the low-conductivity layers. Smaller seepage forces occur in the high-conductivity layers although the flow velocities in these materials are usually larger.

In particular, low-conductivity layers that impede downslope groundwater flow lead to localized areas of high Φ. With a slope-parallel low-conductivity layer acting as a "cap" on the flow system, large outward directed seepage forces occur at the slope toe and lead to high Φ in that region (Figure 12*b*). Vertical or horizontal low-conductivity layers also lead to large hydraulic gradients in the layer. But more importantly, they create an abrupt change in the seepage force direction upslope of the conductivity interface. In both these cases the seepage forces at this interface are directed outward from the slope and a high Φ occurs in this region. In the region upslope of this interface, moderate hydraulic gradients and a higher hydraulic conductivity create larger flow velocities. This corroborates the common observation that discharge areas where springs or seeps exist are prone to slope failure [e.g., *Mathewson et al.*, 1990]. Larger seepage forces occur in the lower-conductivity material, but these are directed laterally in the vertical layer (Figure 13*b*) and vertically in the horizontal layer (Figure 14*b*). When directed laterally, they modify the effective stress field upslope of the vertical layer and induce a larger Φ there. When directed vertically downward, these seepage forces act in the direction of gravitational acceleration and have less effect on the near-surface Φ in the layer.

A number of investigators have used field and modeling studies to demonstrate that hydraulic heterogeneities may control the location of slope failures by causing localized buildup of pore pressures in excess of hydrostatic [e.g., *Patton and Hendron*, 1974; *Hodge and Freeze*, 1977; *Rogers and Selby*, 1980; *Pierson*, 1983; *Rulon and Freeze*, 1985; *Wilson and Dietrich*, 1987; *Reid et al.*, 1988]. These studies typically show that horizontal or slope-parallel layers of contrasting high- and low-conductivity materials found in many geologic settings can lead to pore pressures locally in excess of hydrostatic. Excess pressures commonly occur in the high-conductivity layers that are truncated or confined by surrounding low-conductivity materials. In one example, *Rogers and Selby* [1980] describe failures where higher-conductivity materials were covered by a clayey surface layer of lower conductivity. These landslides initially failed at the toe of the slope. The authors hypothesized that excess pore pressures occurred in the underlying higher-conductivity layer. *Pierson et al.* [1992] note that many shallow slides in Hawaii occur upslope of vertical intrusive dikes and nearly horizontal massive lava flows that apparently have

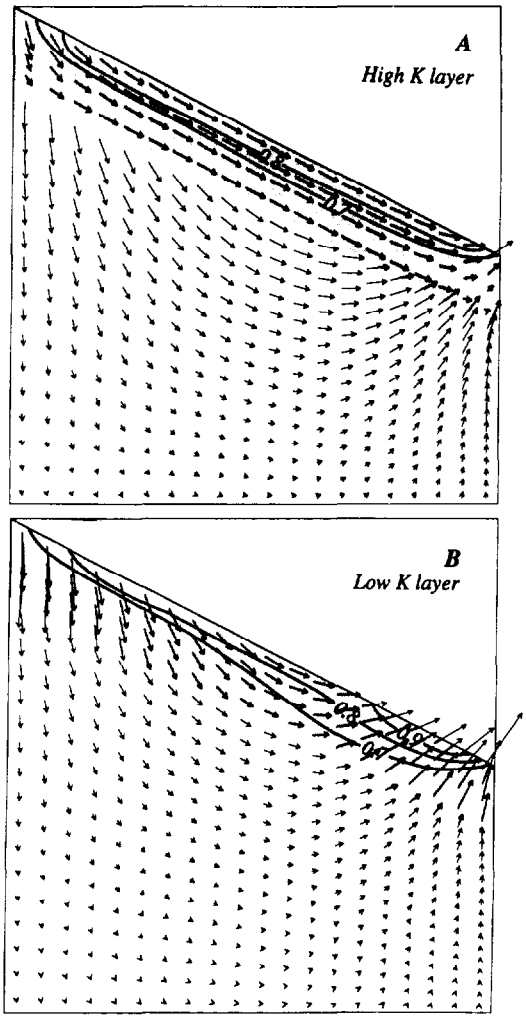

Fig. 12. Normalized seepage force vectors and contours of failure potential Φ greater than 0.7 in a saturated hillslope with a slope-parallel layer. (*a*) Layer has K value 4 orders of magnitude higher than that of surrounding material; (*b*) Layer has K value 5 times lower than that of surrounding material.

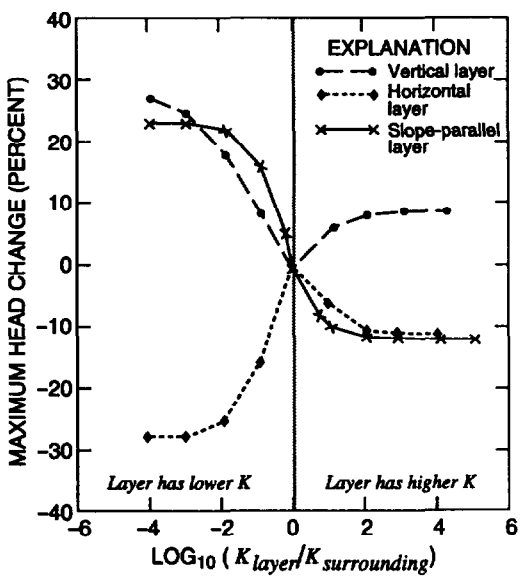

Fig. 11. Maximum percent change in hydraulic head as a function of hydraulic conductivity contrast for the straight, saturated, heterogeneous hillslopes shown in Figure 9. Percent change in head is relative to that in a straight, saturated, homogeneous hillslope.

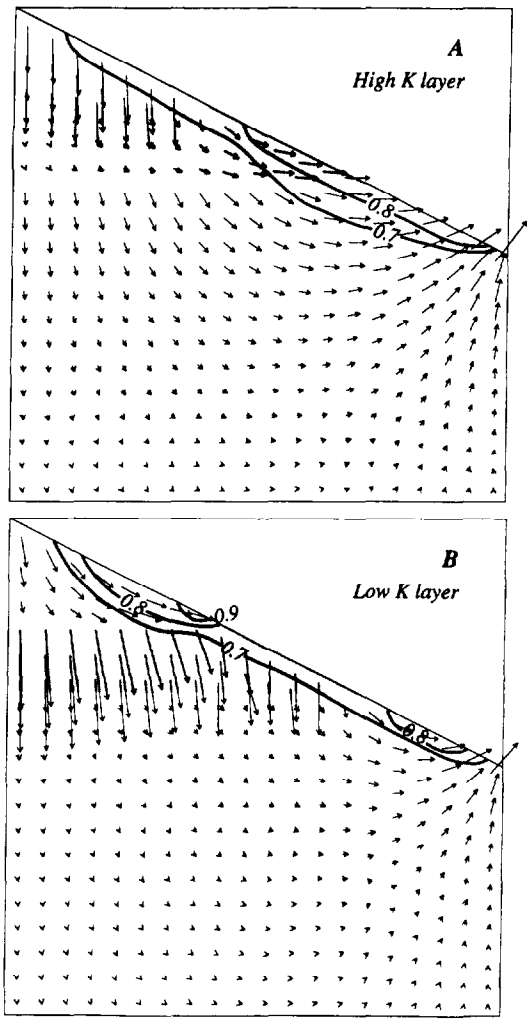

Fig. 13. Normalized seepage force vectors and contours of failure potential Φ greater than 0.7 in a saturated hillslope with a horizontal layer. (*a*) Layer has *K* value 1 order of magnitude higher than that of surrounding material; (*b*) Layer has *K* value 1 order of magnitude lower than that of surrounding material.

low conductivities. Our model results demonstrate how each of these conditions can be destabilizing.

Conclusions

These conclusions are based on our model assumptions and results:

1. Material properties, slope morphology, and hydraulic heterogeneities can each, to some degree, affect the gravity-driven groundwater flow field, seepage force field, effective stress field, and Coulomb failure potential Φ within a saturated hillslope undergoing elastic deformation.

2. In a homogeneous hillslope an increase in Poisson's ratio ν induces more lateral stress in the near-surface region and concomitantly decreases Φ. For typical soils and rocks the value of ν affects the magnitude of Φ, but it has little effect on the change in Φ between dry and saturated conditions.

3. In saturated, homogeneous hillslopes, differences in porosity n have only a small effect on the magnitude and distribution of Φ.

4. Steeper slopes have a larger near-surface Φ. Slope morphology can greatly affect both the groundwater flow field and the magnitude and distribution of Φ. Saturated, convex slopes lead to the largest Φ, which arises where outward directed seepage forces occur in the steeper toe region of the slope.

5. Slope forms with a more uniform near-surface distribution of Φ may be most stable and persistent in landscapes sculpted by landsliding processes. In a dry, homogeneous hillslope, a straight slope form has a more uniform near-surface Φ, whereas in a saturated, homogeneous hillslope, concave and convex-concave slope forms have a more uniform near-surface Φ.

6. Layered materials in a heterogeneous hillslope can greatly affect both the groundwater flow field and the near-surface Φ. Even a small hydraulic conductivity contrast (less than an order of magnitude) reorients the seepage force field. Contrasts of 3 or 4 orders of magnitude have a larger effect. However, contrasts greater than this lead to insignificant further modification of the seepage force field.

7. In a saturated, hydraulically heterogeneous hillslope,

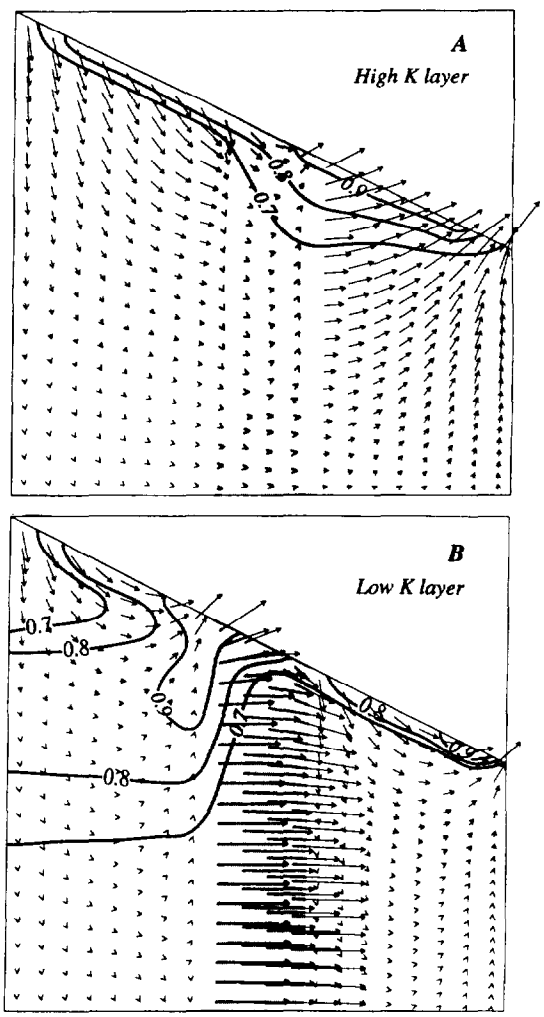

Fig. 14. Normalized seepage force vectors and contours of failure potential Φ greater than 0.7 in a saturated hillslope with a vertical layer. (*a*) Layer has *K* value 4 orders of magnitude higher than that of surrounding material; (*b*) Layer has *K* value 4 orders of magnitude lower than that of surrounding material.

seepage forces are largest in the low-hydraulic-conductivity materials, although flow velocities may be much larger in the high-conductivity materials. Low-conductivity layers that impede downslope flow lead to regions of locally high Φ near the interface with the surrounding high-conductivity material. In these regions, seepage forces are large and directed outward from the slope.

8. In summary, gravity-driven groundwater flow increases the failure potential Φ in near-surface discharge areas where seepage forces are directed outward from the slope. This may occur near the toe of the slope or near a contrasting conductivity interface that impedes flow and extends to the hillslope surface.

Acknowledgments. We thank Rex Baum, John Bredehoeft, and Bill Savage for their helpful reviews of the manuscript.

REFERENCES

Birch, F., Compressibility; elastic constants, *Handbook of Physical Constants*, edited by S. P. Clark, Jr., *Mem. Geol. Soc. Am.*, *97*, 97–173, 1966.

Campbell, R. H., Soil slips, debris flows, and rainstorms in the Santa Monica mountains and vicinity, Southern California, *U.S. Geol. Surv. Prof. Pap.*, *851*, 51 pp., 1975.

Carson, M. A., and M. J. Kirkby, *Hillslope Form and Process*, Cambridge University Press, New York, 1972.

Daly, R. A., G. E. Manger, and S. P. Clark, Jr., Density of rocks, in *Handbook of Physical Constants*, edited by S. P. Clark, Jr., *Mem. Geol. Soc. Am.*, *97*, 19–26, 1966.

Dunn, I. S., L. R. Anderson, and F. W. Kiefer, *Fundamentals of Geotechnical Analysis*, John Wiley, New York, 1980.

Dutton, C. E., *Tertiary History of the Grand Canyon District*, *U.S. Geol. Surv. Monogr.*, vol. 2, 264 pp., U.S. Geological Survey, Washington, D. C., 1882.

Freeze, R. A., and J. A. Cherry, *Groundwater*, Prentice-Hall, Englewood Cliffs, N. J., 1979.

Freeze, R. A., and P. A. Witherspoon, Theoretical analysis of regional groundwater flow, 1, Analytical and numerical solutions to the mathematical model, *Water Resour. Res.*, *2*(4), 641–656, 1966.

Freeze, R. A., and P. A. Witherspoon, Theoretical analysis of regional groundwater flow, 2, Effect of water-table configuration and subsurface permeability variation, *Water Resour. Res.*, *3*(2), 623–634, 1967.

Gerber, E., and A. E. Scheidegger, Stress-induced weathering of rock masses, *Eclogae Geol. Helv.*, *62*(2), 401–415, 1969.

Gerber, E., and A. E. Scheidegger, Geomorphological evidence for the geophysical stress field in mountain massifs, *Riv. Ital. Geofis.*, *2*, 47–52, 1975.

Hodge, R. A., and R. A. Freeze, Groundwater flow systems and slope stability, *Can. Geotech. J.*, *14*, 466–476, 1977.

Iverson, R. M., and J. J. Major, Rainfall, ground-water flow and seasonal movement at Minor Creek landslide, northwestern California: Physical interpretation of empirical relations, *Geol. Soc. Am. Bull.*, *99*, 579–594, 1987.

Iverson, R. M., and M. E. Reid, Gravity-driven groundwater flow and slope failure potential, 1, Elastic effective stress model, *Water Resour. Res.*, this issue.

Jaeger, J. C., and N. G. W. Cook, *Fundamentals of Rock Mechanics*, 3rd ed., Chapman and Hall, New York, 1979.

Kelsey, H. M., Formation of inner gorges, *Catena*, *15*, 433–458, 1988.

Kirkby, M. J., Hillslope process-response models based on the continuity equation, in *Slopes, Form and Process*, *Spec. Publ.*, vol. 3, edited by D. Brunsden, pp. 15–30, Institution of British Geographers, London, 1971.

Lambe, T. W., and R. V. Whitman, *Soil Mechanics*, SI Version, John Wiley, New York, 1979.

Mathewson, C. C., J. R. Keaton, and P. M. Santi, Role of bedrock ground water in the initiation of debris flows and sustained post-flow stream discharge, *Bull. Assoc. Eng. Geol.*, *27*, 73–83, 1990.

McTigue, D. F., and C. C. Mei, Gravity-induced stresses near topography of small slope, *J. Geophys. Res.*, *86*(B10), 9268–9278, 1981.

Patton, F. D., and A. J. Hendron, General report on mass movements, *Proceedings of the 2nd International Congress of the International Association of Engineering Geologists, Sao Paulo, Brazil*, vol. 2, pp. V-GR-1–V-GR-57, 1974.

Pierson, T. C., Soil pipes and slope stability, *Q. J. Eng. Geol.*, *16*, 1–11, 1983.

Pierson, T. C., S. D. Ellen, and R. M. Iverson, Shallow landsliding during intense rainfall, Oahu, Hawaii, in *Proceedings of the Sixth International Symposium on Landslides*, Balkeema, Rotterdam, Netherlands, in press, 1992.

Reid, M. E., H. P. Nielsen, and S. J. Dreiss, Hydrologic factors triggering a shallow hillslope failure, *Bull. Assoc. Eng. Geol.*, *25*(3), 349–361, 1988.

Rogers, N. W., and M. J. Selby, Mechanisms of shallow translational landsliding during summer rainstorms in New Zealand, *Geogr. Ann.*, *62A*(1–2), 11–21, 1980.

Rulon, J. J., and R. A. Freeze, Multiple seepage faces on layered slopes and their implications for slope-stability analysis, *Can. Geotech. J.*, *22*, 347–356, 1985.

Skempton, A. W., and F. A. DeLory, Stability of natural slopes in London clay, *Proc. Int. Conf. Soil Mech. Found. Eng.*, *4th*, *Engng*, 378–381, 1957.

Wilson, C. J., and W. E. Dietrich, The contribution of bedrock groundwater flow to storm runoff and high pore pressure in hollows, *Erosion and Sedimentation in the Pacific Rim*, *Int. Assoc. Hydrol. Sci. Publ.*, *165*, 49–59, 1987.

R. M. Iverson, U.S. Geological Survey, Cascades Volcano Observatory, 5400 MacArthur Blvd., Vancouver, WA 98661.

M. E. Reid, U.S. Geological Survey, 677 Ala Moana Blvd., Suite 415, Honolulu, HI 96813.

(Received January 24, 1991;
revised October 16, 1991;
accepted October 25, 1991.)